



OPEN

## Insight into the heat transfer of third-grade micropolar fluid over an exponentially stretched surface

Kamel Guedri<sup>1</sup>, N. Ameer Ahammad<sup>2</sup>, Sohail Nadeem<sup>3</sup>, ElSayed M. Tag-ELDin<sup>4</sup>, Aziz Ullah Awan<sup>5</sup>✉ & Mansour F. Yassen<sup>6,7</sup>

Due to their unique microstructures, micropolar fluids have attracted enormous attention for their industrial applications, including convective heat and mass transfer polymer production and rigid and random cooling particles of metallic sheets. The thermodynamical demonstration is an integral asset for anticipating the ideal softening of heat transfer. This is because there is a decent connection between mathematical and scientific heat transfers through thermodynamic anticipated outcomes. A model is developed under the micropolar stream of a non-Newtonian (3rd grade) liquid in light of specific presumptions. Such a model is dealt with by summoning likeness answers for administering conditions. The acquired arrangement of nonlinear conditions is mathematically settled using the fourth-fifth order Runge-Kutta-Fehlberg strategy. The outcomes of recognized boundaries on liquid streams are investigated in subtleties through the sketched realistic images. Actual amounts like Nusselt number, Sherwood number, and skin-part coefficient are explored mathematically by tables. It is observed that the velocity distribution boosts for larger values of any of  $\alpha_1$ ,  $\beta$ , and declines for larger  $\alpha_2$  and Hartmann numbers. Furthermore, the temperature distribution  $\theta(\eta)$  shows direct behavior with the radiation parameter and Eckert number, while, opposite behavior with  $Pr$ , and  $K$ . Moreover, the concentration distribution shows diminishing behavior as we put the higher value of the Brownian motion number.

Many researchers around the globe are showing a keen interest in learning more about the non-Newtonian fluid flow. The motivation for studying these fluids is their potential usage in industries and technology. These fluids have paramount prominence in material processing, bioengineering, geophysics, oil reservoir engineering, chemical, nuclear, and many other fields. Many materials of our daily life use, such as apple sauce, mud, paints, shampoos, soaps, ice cream, condensed milk, polymeric liquids, low shear rate blood, pasta, oils, etc., show a highly complex nature and are taken as non-Newtonian liquids. Rheological physical attributes of a non-Newtonian fluid are impossible to explore by using the simple Navier-Stokes theory (unlike for viscid fluids). The third-grade fluid is one of the categories of differential type fluids. It describes shear thinning and thickening properties. Abbasbandy et al.<sup>1</sup> analyzed both exact and series solutions for third-grade fluid using thin film. Hayat et al.<sup>2</sup> scrutinized rotating third-grade MHD fluid flow bounded between two permeable sheets. Farooq et al.<sup>3</sup> probed mass and thermic transmission for third-grade fluid inside a vertically positioned flow configuration besides viscous dissipation. Sinha<sup>4</sup> studied MHD third-grade fluid flow inside a pipe having stretched and porous walls. Okoya<sup>5</sup> examined the heat-exchange properties of an exothermic reactive third-grade fluid across a circular passage by considering the Reynolds viscosity model and its uses in the processing industries. Hayat et al.<sup>6</sup> explored MHD third-grade fluid flow bounded with convective heated and stretched surfaces. Magneto hydrodynamic stagnation

<sup>1</sup>Mechanical Engineering Department, College of Engineering and Islamic Architecture, Umm Al-Qura University, P.O. Box 5555, Makkah 21955, Saudi Arabia. <sup>2</sup>Department of Mathematics, Faculty of Science, University of Tabuk, P.O. Box 741, Tabuk 71491, Saudi Arabia. <sup>3</sup>Department of Mathematics, Quaid-i-Azam University, Islamabad 45320, Pakistan. <sup>4</sup>Faculty of Engineering and Technology, Future University in Egypt, New Cairo 11835, Egypt. <sup>5</sup>Department of Mathematics, University of the Punjab, Lahore 54590, Pakistan. <sup>6</sup>Department of Mathematics, College of Science and Humanities in Al-Aflaj, Prince Sattam Bin Abdulaziz University, Al-Aflaj 11912, Saudi Arabia. <sup>7</sup>Department of Mathematics, Faculty of Science, Damietta University, New Damietta 34517, Damietta, Egypt. ✉email: aziz.math@pu.edu.pk

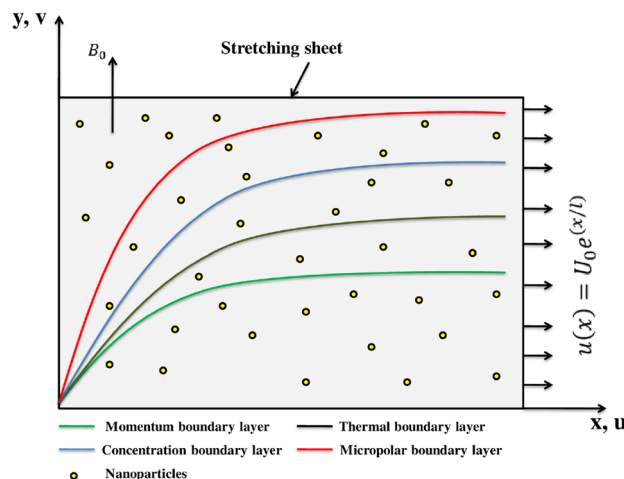


**Figure 1.** Flow geometry.

point flow for non-Newtonian (third-grade) fluid caused by the non-linearly stretchy surface is examined by Hayat et al.<sup>7</sup>. Interested readers can see some recent work on third-grade fluids here<sup>8–11</sup>.

Eringen<sup>12</sup> was the pioneer who studied the flow of micropolar fluids. Physical examples of micropolar fluids can be seen in ferrofluids, blood flows, bubbly liquids, liquid crystals, and so on, all of them containing intrinsic polarities. Eringen's hypothesis<sup>12</sup> proclaims that any fluid formed from rigid, arbitrarily oriented, or spherical particles with particular micro-rotations is called the micropolar fluid. Guram and Smith<sup>13</sup> studied flow subject to stagnation point for a micropolar liquid model. The flow model of a micropolar liquid caused by a heat source over an axisymmetric and rotating sheet is probed by Gorla and Takhar<sup>14</sup>. By considering combined convective conditions, Gorla et al.<sup>15</sup> presented an axisymmetric stagnation point stream through a perpendicular standing cylinder for micropolar fluid. MHD effects on micropolar liquid stream across a continually moving plate were investigated by Sadeek<sup>16</sup>. Eldahab et al.<sup>17</sup> probed the influence of radiations on thermal transmission for a micropolar liquid stream across a flat sheet in a permeable medium. Mohamed and Abo-Dahab<sup>18</sup> deliberated the consequences of thermal radiations and chemical reactions on mass and thermal transport for micropolar fluid in penetrable media. Investigation for the micropolar fluid flow due to permeable stretched sheet also consequent thermal transmission is done by Turkyilmazoglu<sup>19</sup>. The darcy-Forchheimer flow of 3D micropolar fluid along horizontal parallel sheets in the revolving system in a penetrable medium is analyzed by Khan et al.<sup>20</sup>. For an in-depth investigation of micropolar fluid flow, we refer the curious reader to some recent studies<sup>21–25</sup>.

Over the decade, stream due to the extendable sheet has acquired astonishing significance among scientists due to its modern design execution. Not many of these applications incorporate hot rolling, paper production, glass blowing, polymer and metal expulsion, and precious stone development. Crane<sup>26</sup> introduced the investigation of stream subject to an extended sheet. Brady and Acrivos<sup>27</sup> concentrated on the liquid stream in an extended channel. Specialists observed that an answer for a particular worth of Reynolds number exists for a 2D stream. Ahmad et al.<sup>28</sup> performed the computational investigation of an unstable (3-D) chemically reacting MHD flow of Maxwell fluid. Ahmad et al.<sup>29</sup> used the Cattaneo-Christov thermal influx model to probe the hybrid Micropolar nanoliquid stream with triple stratification. Many researchers have investigated heat and thermal investigation of fluids over stretched surfaces<sup>30–36</sup>. Khan et al.<sup>37</sup> explored the MHD stream of second-grade fluid with multiple slip constraints. The non-Newtonian fluid has been widely discussed by<sup>38–42</sup>.

The above-cited literature review shows that little attention is paid to the study considering the effects of third-grade micropolar fluid flow over an expanding surface. Motivated by the numerous uses of non-Newtonian fluids and nanofluids<sup>43–49</sup>, a third-grade micropolar liquid stream subject to a stretching sheet is investigated here. The primary purpose of this extensive study is to improve thermal transportation subject to the existence of micro-rotations of tiny nanoparticles. The numerical plan is made in the approaching segment by utilizing liquid stream presumptions. With the utilization of likeness changes, an arrangement of PDEs is decreased into a non-straight arrangement of ODEs. The mathematical strategy RK45 is used to settle the acquired framework systematically. The influence of some pertinent parameters is spotlighted on each temperature field  $\theta(\eta)$ , concentration field  $\phi(\eta)$ , velocity field  $f'(\eta)$ , and micropolar field  $h(\eta)$  through graphical representations Figs. 2, 3, 4, 5, 6, 7, 8, 9, 10, 11, 12, 13. Tables 1, 2, 3 help understand the numeric variance of skin-friction coefficient, Nusselt and Sherwood number caused by involved parameters. This report is related to various applications in manufacturing plastic and metal spinning, paints, liquids material, crude oil purification, heat exchangers, polymer extrusion, etc.

### Flow analysis

Steady incompressible and 2D stream of micropolar liquid over an extendable sheet is to be investigated in this communication. The  $x$ -axis is supposed along the continuously expanded surface while  $y$ -axis is taken perpendicular to this assumed surface in upward direction to the fluid (See Fig. 1). For the third grade fluid, the stress tensor is as follows:

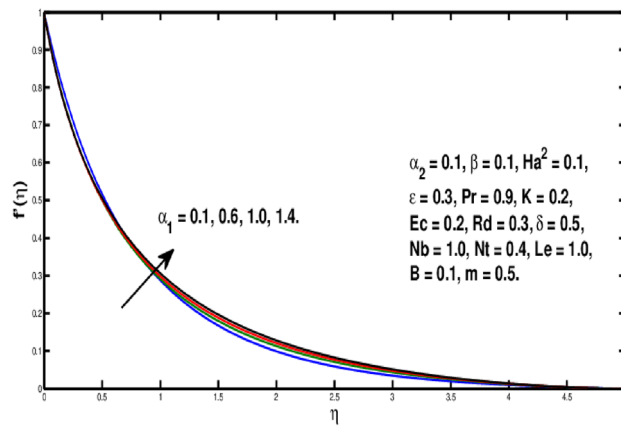


Figure 2. Variation of  $\alpha_1$  on  $f'(\eta)$ .

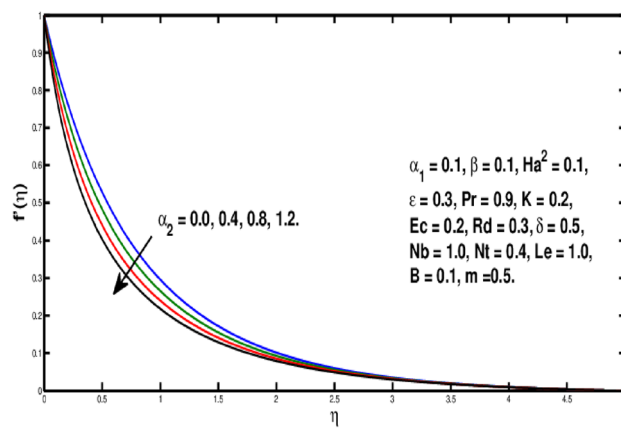


Figure 3. Variation of  $\alpha_2$  on  $f'(\eta)$ .

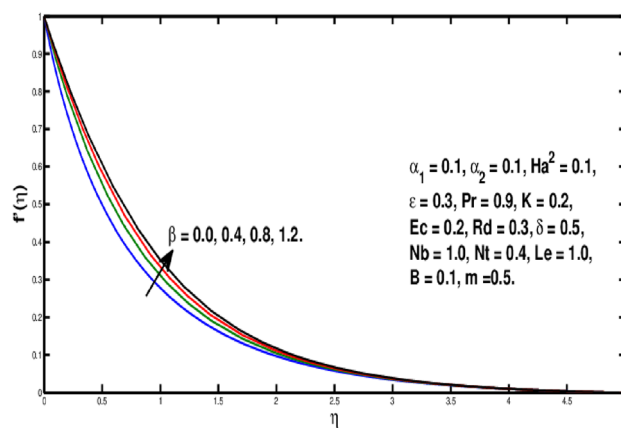


Figure 4. Variation of  $\beta$  on  $f'(\eta)$ .

$$\mathbf{T} = -p\mathbf{I} + \mu\mathbf{B}_1 + \alpha_1^*\mathbf{B}_2 + \alpha_2^*\mathbf{B}_1^2 + \beta_1\mathbf{B}_3 + \beta_2(\mathbf{B}_1\mathbf{B}_2 + \mathbf{B}_2\mathbf{B}_1) + \beta_3\mathbf{B}_1(\text{trc}\mathbf{B}_1^2).$$

Here  $p$ ,  $\mathbf{I}$ ,  $\mathbf{T}$ , and  $\mathbf{S}$  are the pressure, identity tensor, Cauchy stress tensor, and the extra stress tensor respectively. Furthermore,  $\alpha_k^*$  ( $k = 1, 2$ ),  $\beta_j$  ( $j = 1, 2, 3$ ) are metallic constants and  $\mathbf{B}_i$  ( $i = 1, 2, 3$ ) are the kinematic tensors defines as:

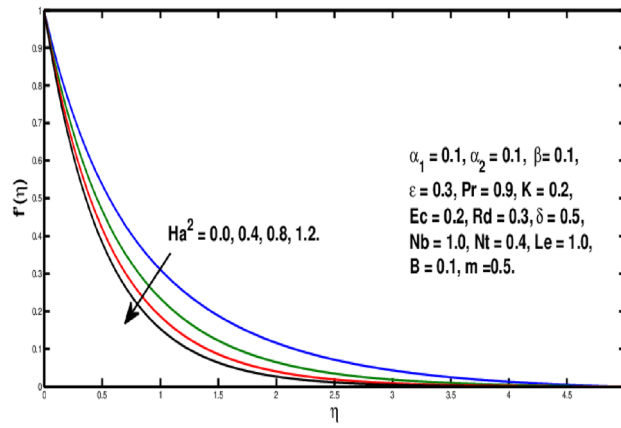


Figure 5. Variation of  $Ha^2$  on  $f'(\eta)$ .

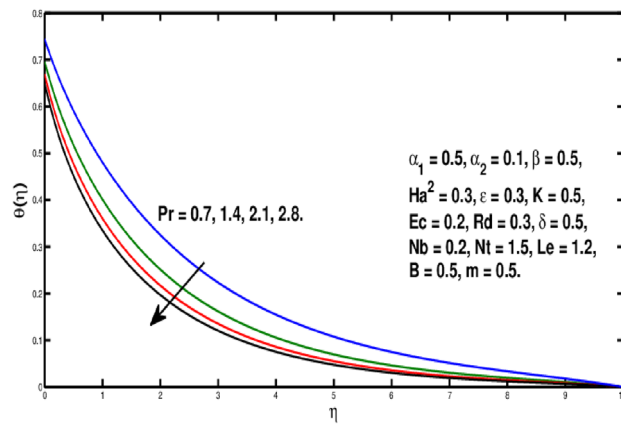


Figure 6. Variation of  $Pr$  on  $\theta(\eta)$ .

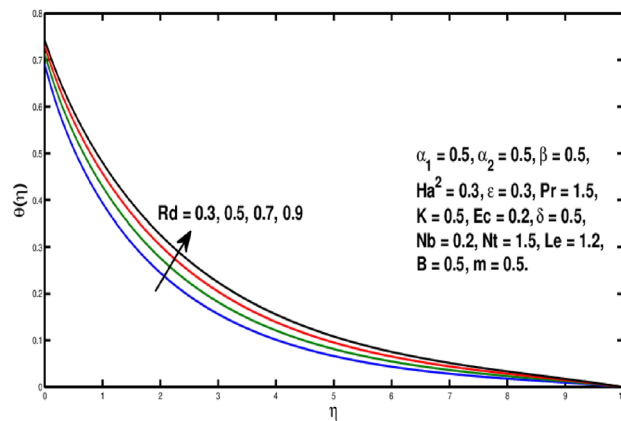


Figure 7. Variation of  $Rd$  on  $\theta(\eta)$ .

$$\mathbf{B}_1 = (\mathbf{L})^T + \mathbf{L},$$

$$\mathbf{B}_n = \frac{D\mathbf{B}_{n-1}}{Dt} + \mathbf{B}_{n-1}\mathbf{L} + (\mathbf{L})^T\mathbf{B}_{n-1}, \quad n = 2, 3$$

where,  $\mathbf{L} = \nabla\mathbf{V}$ .

Using the boundary layer estimations<sup>50–53</sup> in case of 3rd-grade fluid, notably, inside boundary layer  $\frac{\partial p}{\partial x}$ ,  $\frac{\partial^2 u}{\partial x^2}$ ,  $\frac{\partial u}{\partial x}$ , and  $u$  are  $O(1)$ ,  $v$  and  $y$  are  $O(\delta)$ ,  $\frac{\alpha_j}{\rho}$  ( $j = 1, 2$ ) and  $v$  be  $O(\delta^2)$ , and  $\frac{\beta_k}{\rho}$  ( $k = 1, 2, 3$ ) being  $O(\delta^4)$  as well as the

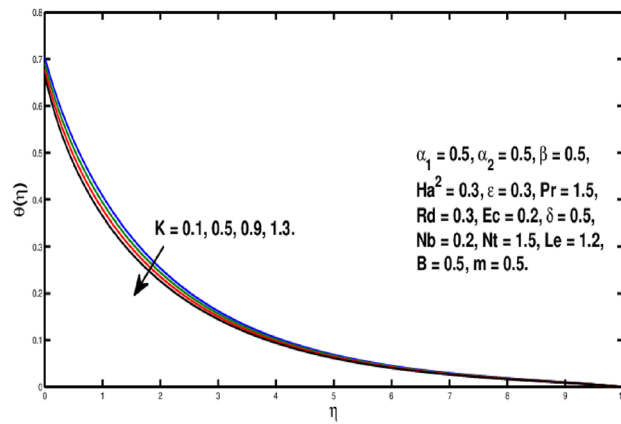


**Figure 8.** Variation of  $K$  on  $\theta(\eta)$ .

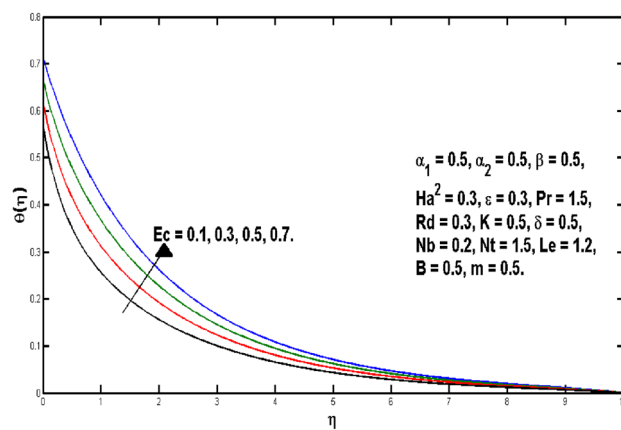


**Figure 9.** Variation of  $Ec$  on  $\theta(\eta)$ .

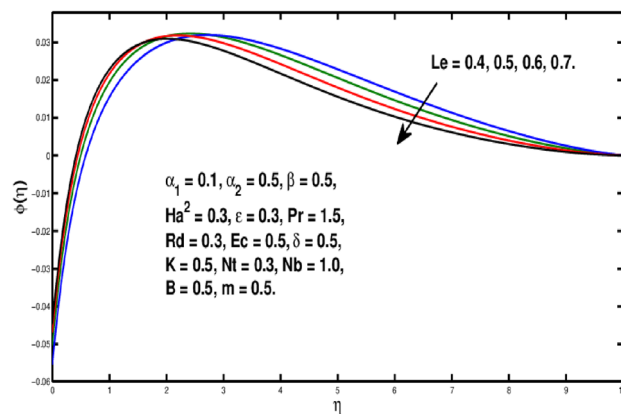


**Figure 10.** Variation of  $Le$  on  $\phi(\eta)$ .

components of  $O(\delta)$  are ignored ( $\delta$  is boundary layer width), the mathematical model for the said flow is as follows:

$$\frac{\partial v}{\partial y} + \frac{\partial u}{\partial x} = 0, \tag{1}$$

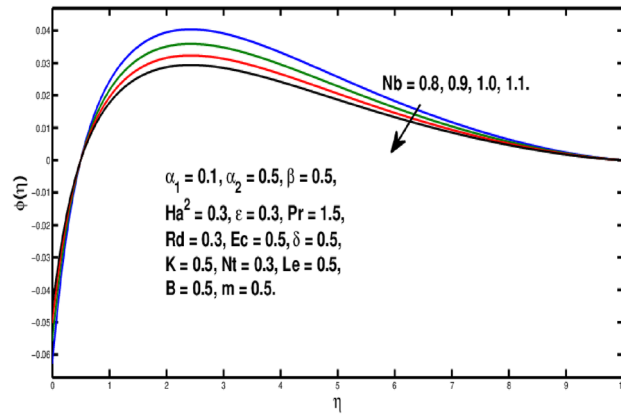


Figure 11. Variation of  $Nb$  on  $\phi(\eta)$ .

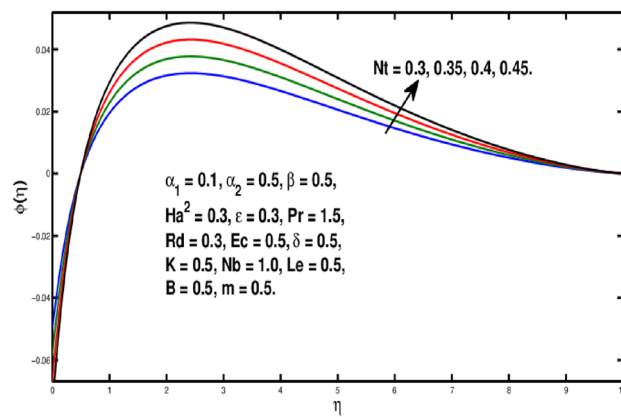


Figure 12. Variation of  $Nt$  on  $\phi(\eta)$ .

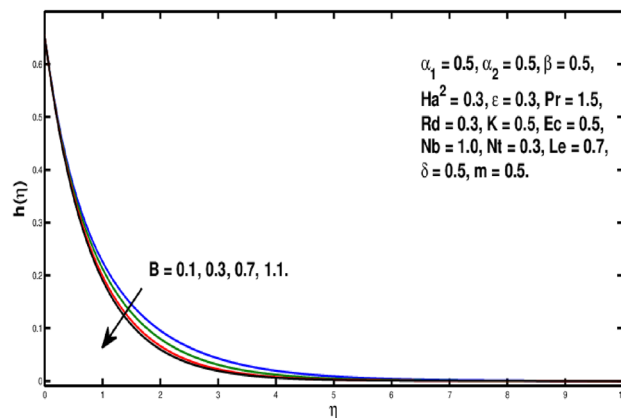


Figure 13. Variation of  $B$  on  $h(\eta)$ .

$$\begin{aligned}
 v \frac{\partial u}{\partial y} + u \frac{\partial u}{\partial x} = & \frac{\alpha_1^*}{\rho} \left( \frac{\partial u}{\partial x} \frac{\partial^2 u}{\partial y^2} + u \frac{\partial^3 u}{\partial x \partial y^2} + 3 \frac{\partial u}{\partial y} \frac{\partial^2 v}{\partial y^2} + v \frac{\partial^3 u}{\partial y^3} \right) + 2 \frac{\alpha_2^*}{\rho} \frac{\partial u}{\partial y} \frac{\partial^2 v}{\partial y^2} \\
 & + 6 \frac{\beta_3}{\rho} \left( \frac{\partial u}{\partial y} \right)^2 \frac{\partial^2 u}{\partial y^2} + \left( \nu + \frac{k}{\rho} \right) \frac{\partial^2 u}{\partial y^2} + \frac{k}{\rho} \frac{\partial N}{\partial y} - \frac{\sigma B_0^2}{\rho} u,
 \end{aligned}
 \tag{2}$$

$\alpha_1$	$\alpha_2$	$\beta$	$Ha^2$	$\frac{1}{\sqrt{2}}\sqrt{Re_x}Cf_x$
0.1	0.5	0.5	0.3	-1.7445
0.3				-2.8171
0.5				-3.9383
0.7				-5.0724
0.1	0.1			-1.5369
	0.3			-1.6391
	0.5			-1.7445
	0.7			-1.8523
	0.5	0.1		-2.3654
		0.3		-1.9467
		0.5		-1.7445
		0.7		-1.6153
		0.5	0.1	-1.6381
			0.2	-1.6943
			0.3	-1.7445
			0.4	-1.7902

**Table 1.** Variation of skin friction coefficient with  $\alpha_1, \alpha_2, \beta$ , and  $Ha^2$ .

$\epsilon$	$Pr$	$K$	$Ec$	$Rd$	$\delta$	$Nb$	$Nt$	$\sqrt{\frac{2}{X}}\frac{Nu_x}{\sqrt{Re_x}}$
0.2	1.5	0.2	0.8	0.5	0.5	1.0	0.3	0.9230
0.25								0.9205
0.3								0.9180
0.35								0.9155
0.3	0.7							0.7210
	1.1							0.8393
	1.5							0.9180
	2.1							0.9971
	1.5	0.2						0.9180
		0.25						0.9346
		0.3						0.9513
		0.35						0.9680
		0.2	0.2					0.6247
			0.4					0.7211
			0.6					0.8189
			0.8					0.9180
			0.8	0.2				0.8362
				0.3				0.8633
				0.4				0.8907
				0.5				0.9180
				0.5	0.4			0.8822
					0.45			0.9009
					0.5			0.9180
					0.55			0.9337
					0.5	0.9		0.9180
						1.0		0.9180
						1.1		0.9180
						1.2		0.9180
						1.0	0.2	0.9175
							0.3	0.9180
							0.4	0.9185
							0.5	0.9190

**Table 2.** Variation of Nusselt number with  $\epsilon, Pr, K, Ec, Rd, \delta, Nb$ , and  $Nt$ .

$Le$	$Nb$	$Nt$	$\sqrt{\frac{2}{x}} \frac{Sh_x}{\sqrt{Re_x}}$
0.2	1.0	0.3	-0.1650
0.5			-0.1652
0.8			-0.1653
1.1			-0.1654
0.7	0.9		-0.1836
	1.0		-0.1652
	1.1		-0.1502
	1.2		-0.1377
	1.0	0.2	-0.1101
		0.3	-0.1652
		0.4	-0.2204
		0.5	-0.2757

**Table 3.** Variation of Sherwood number with  $Le$ ,  $Nb$ , and  $Nt$ .

$$v \frac{\partial T}{\partial y} + u \frac{\partial T}{\partial x} = \frac{(\mu + k)}{(\rho C_p)_f} \left( \frac{\partial u}{\partial y} \right)^2 + \frac{Q}{(\rho C_p)_f} (T - T_\infty) - \frac{1}{(\rho C_p)_f} \frac{\partial q_r}{\partial y} + \frac{1}{(\rho C_p)_f} \frac{\partial}{\partial y} \left( k_1(T) \frac{\partial T}{\partial y} \right) + \tau \left( \frac{D_T}{T_\infty} \left( \frac{\partial T}{\partial y} \right)^2 + D_B \frac{\partial T}{\partial y} \frac{\partial C}{\partial y} \right), \tag{3}$$

$$u \frac{\partial \hat{C}}{\partial x} + v \frac{\partial \hat{C}}{\partial y} = D_B \frac{\partial^2 \hat{C}}{\partial y^2} + \left( \frac{\partial^2 T}{\partial y^2} \right) \frac{D_T}{T_\infty}, \tag{4}$$

$$u \frac{\partial \hat{N}}{\partial x} + v \frac{\partial \hat{N}}{\partial y} = \frac{\partial^2 \hat{N}}{\partial y^2} \left( \frac{\gamma}{\rho j} \right) - \frac{k}{j \rho} \left( 2\hat{N} + \frac{\partial u}{\partial y} \right), \tag{5}$$

subjected to the boundary conditions

$$\begin{cases} N = -m \frac{\partial u}{\partial y}, & u = U_0 \exp(x/l), & T_f + h_f \left( \frac{\partial T}{\partial y} \right) = T, & v = 0, & \frac{D_T}{T_\infty} \frac{\partial T}{\partial y} + D_B \frac{\partial C}{\partial y} = 0, & \text{as } y = 0, \\ N \rightarrow 0, & u \rightarrow 0, & \hat{C} \rightarrow \hat{C}_\infty, & T \rightarrow T_\infty, & & \text{as } y \rightarrow \infty, \end{cases} \tag{6}$$

where  $v$  and  $u$  are the parts of velocity in  $y$  and  $x$  directions respectively.  $\hat{C}$  denotes concentration,  $N$  being Part of microrotation vector, orthogonal to the considered plane, and  $\rho$  is density of fluid.  $D_T$  shows thermophoresis diffusion coefficient,  $D_B$  is Brownian diffusion coefficient, and  $\tau = \frac{(\rho C_p)_{nf}}{(\rho C_p)_f}$  is the quotient of the heat capacity of the nano-particles and the heat of base fluid.  $C_\infty$  and  $T_\infty$  are free stream concentration and temperature.  $\mu$  denotes dynamic viscosity whereas  $\nu = \frac{\mu}{\rho}$  represents kinematic viscosity,  $C_p$  is specific heat,  $T$  for temperature,  $\gamma$  shows spin gradient viscosity,  $k_1(T)$  is variable thermal conductivity,  $j$  is microinertia density,  $k_f$  is thermal conductivity of base fluid,  $k$  is the vortex viscosity, and  $(\alpha_1^*, \alpha_2^*, \beta_3)$  are material constants. Taking  $\gamma$  as

$$\gamma = \left( \frac{k}{2} + \mu \right) j = \left( 1 + \frac{K}{2} \right) \mu j, \tag{7}$$

and define  $K = \frac{k}{\mu}$  as micropolar parameter.

Also, suppose that

$$k_1(T) = k_f (1 + \epsilon \theta(\eta)). \tag{8}$$

The Rosseland radiative heat flux is  $q_r = \frac{-4\sigma^*}{3k^*} \frac{\partial^2 T}{\partial y^2} \approx 4T_\infty^3 T - 3T_\infty^4$ , where mean absorption coefficient is shown as  $k^*$  and  $\sigma^*$  represents Stefan-Boltzmann constant.

$$\frac{\partial q_r}{\partial y} = \frac{-16T_\infty^3 \sigma^*}{3k^*} \frac{\partial^2 T}{\partial y^2}. \tag{9}$$

Equation (3) is now transformed as



$$\begin{aligned}
 v \frac{\partial T}{\partial y} + u \frac{\partial T}{\partial x} &= \frac{(k + \mu)}{(C_p \rho)_f} \left( \frac{\partial u}{\partial y} \right)^2 + \frac{1}{(\rho C_p)_f} \frac{16T_\infty^3 \sigma^*}{3k^*} \frac{\partial^2 T}{\partial y^2} + \tau \left( D_B \frac{\partial C}{\partial y} \frac{\partial T}{\partial y} + \left( \frac{\partial T}{\partial y} \right)^2 \frac{D_T}{T_\infty} \right) \\
 &+ \frac{1}{(\rho C_p)_f} \frac{\partial}{\partial y} \left( \frac{\partial T}{\partial y} k_1(T) \right) + \frac{Q}{(\rho C_p)_f} (T - T_\infty).
 \end{aligned}
 \tag{10}$$

Defining the similarity variables  $h, f, \eta,$  and  $\theta$  as:

$$\begin{cases} \psi(x, y) = \sqrt{2vlU_0} \exp\left(\frac{x}{2l}\right) f(\eta), & N = U_0 \sqrt{\frac{U_0}{2vl}} \exp\left(\frac{3x}{2l}\right) h(\eta), \\ \phi(\eta) = \frac{C - C_\infty}{C_f - C_\infty}, & \theta(\eta) = \frac{T - T_\infty}{T_f - T_\infty}, & \eta = \sqrt{\frac{U_0}{2vl}} \exp\left(\frac{x}{2l}\right) y, \end{cases}
 \tag{11}$$

where  $\psi(x, y)$  is the stream function.

$$u = \frac{\partial \psi}{\partial y} = U_0 \exp\left(\frac{x}{l}\right) f'(\eta), \quad \text{and} \quad v = -\frac{\partial \psi}{\partial x} = -\sqrt{\frac{vU_0}{2l}} \exp\left(\frac{x}{2l}\right) (f + \eta f'),$$

$\eta$  is similar variable, while  $\theta(\eta), f'(\eta)$  and  $\phi(\eta)$  are the similarity representation of temperature, velocity profile, and concentration.  $h(\eta)$  is dimensionless micropolar profile respectively. Furthermore,  $T_f$  and  $C_f$  represent the temperature and concentration at the wall of the sheet, respectively. Mass conservation equation is automatically satisfied by putting Eq. (11) in Eq. (1). The PDEs (2), (4), (5), and (10) are transmuted to the non-linear coupled ODEs:

$$\begin{aligned}
 (1 + K)f''' + f''f + \alpha_1 \left[ -ff^{(iv)} - 2\eta f'''f'' - 9(f'')^2 + 3f'''f' \right] - \alpha_2 \left[ 3(f'')^2 + \eta f'''f'' \right] \\
 + 3\beta(f'')^2 f''' - 2Ha^2 f' - 2(f')^2 = 0,
 \end{aligned}
 \tag{12}$$

$$\frac{1}{Pr} \left[ \epsilon(\theta')^2 + \theta'' + \epsilon\theta\theta'' \right] + f\theta' + (1 + K)Ec(f'')^2 + \frac{4}{3}Rd\theta'' + \delta\theta + (\theta')^2 Nt + \theta'\phi'Nb = 0,
 \tag{13}$$

$$\left( \frac{Nt}{Nb} \right) \theta'' + \phi'' + Lef\phi' = 0,
 \tag{14}$$

$$fh' + \left( 1 + \frac{K}{2} \right) h'' - 3hf' - 2KB(f'' + 2h) = 0.
 \tag{15}$$

With the altered BCs as:

$$\begin{cases} f'(\infty) = 0, & f''(\infty) = 0, & f(0) = 0, & f'(0) = 1, \\ h(\infty) = 0, & \phi(\infty) = 0, & \theta'(0)Nt + \phi'(0)Nb = 0, \\ \theta(\infty) = 0, & \theta(0) = 1 + \delta_T\theta'(0), & h(0) = -mf''(0). \end{cases}
 \tag{16}$$

Here involved dimensionless variables are given as

$$\begin{cases} \alpha_1 = \frac{U_0}{\rho\nu l} \alpha_1^* \exp\left(\frac{x}{l}\right), & \alpha_2 = \frac{U_0}{\rho\nu l} \alpha_2^* \exp\left(\frac{x}{l}\right), & \beta = \frac{U_0^3}{\rho\nu^2 l} \beta_3 \exp\left(\frac{3x}{l}\right), & Ha^2 = \frac{\sigma B_0^2 l}{\rho U_0} \exp(-x/l), \\ Pr = \frac{\mu C_p}{k_f}, & K = \frac{k}{\mu}, & Nb = \frac{\tau D_B}{\nu} (\widehat{C}_f - \widehat{C}_\infty), & Le = \frac{\nu}{D_B}, \\ Nt = \frac{\tau D_T}{\nu T_\infty} (T_f - T_\infty), & B = \frac{\nu l}{U_0} \exp(-x/l), & \delta = \frac{2lQ}{U_0} \exp\left(\frac{l}{x}\right), & Rd = \frac{4T_\infty^3 \sigma^*}{\mu k^* C_p}, \\ Ec = \frac{U_0^2}{C_p(T_f - T_\infty)} \exp\left(\frac{2x}{l}\right), & \delta_T = h_f \sqrt{\frac{U_0}{2vl}} \exp\left(\frac{x}{2l}\right), \end{cases}
 \tag{17}$$

where  $\delta_T$  is thermal slip,  $B$  is microinertia density parameter,  $Ec, Pr, Ha^2$  and  $Le$  are Eckert, Prandtl, Hartmann, and Lewis number respectively,  $Nt$  is Thermophoresis parameter,  $Nb$  is Brownian motion parameter,  $K$  the micropolar parameter,  $\delta$  is the heat generation/absorption parameter,  $Rd$  the radiation parameter,  $\beta, \alpha_1$  and  $\alpha_2$  are 3rd grade, cross viscous and viscoelastic parameter.

The local Sherwood number  $Sh_x,$  skin friction coefficient  $Cf_x$  and local Nusselt number  $Nu_x$  are

$$Sh_x = \frac{xj_w}{D_B(\widehat{C}_f - \widehat{C}_\infty)}, \quad Cf_x = \frac{\tau_w}{\rho U_w^2}, \quad Nu_x = \frac{xq_w}{k_f(T_f - T_\infty)},
 \tag{18}$$

where

$$j_w = -D_B \left( \frac{\partial C}{\partial y} \right) \Big|_{y=0},
 \tag{19}$$

$$\tau_w = \left[ k\hat{N} + (k + \mu) \frac{\partial u}{\partial y} + 2\beta_3 \left( \frac{\partial u}{\partial y} \right)^3 + \alpha_1^* \left( v \frac{\partial^2 u}{\partial y^2} + u \frac{\partial^2 u}{\partial y \partial x} + 2 \frac{\partial u}{\partial x} \frac{\partial u}{\partial y} \right) \right]_{y=0}, \tag{20}$$

$$q_w = - \left( k_f + \frac{16T_\infty^3 \sigma^*}{3k^*} \right) \frac{\partial T}{\partial y} \Big|_{y=0}. \tag{21}$$

The above expressions in the form of similarity variables are:

$$\frac{1}{\sqrt{2}} \sqrt{Re_x} Cf_x = \left[ (K + 1)f''(\eta) + \alpha_1 \left( \frac{7}{2} f''(\eta) f'(\eta) - \frac{1}{2} f(\eta) f'''(\eta) \right) + \beta (f''(\eta))^3 + Kh(\eta) \right]_{\eta=0}, \tag{22}$$

$$\sqrt{\frac{2}{X}} \frac{Nu_x}{\sqrt{Re_x}} = - \left( 1 + \frac{4}{3} Rd \right) \theta'(0), \tag{23}$$

$$\sqrt{\frac{2}{X}} \frac{Sh_x}{\sqrt{Re_x}} = -\phi'(0), \tag{24}$$

where  $X = \frac{x}{l}$  and  $Re_x = \frac{U_w(x)x}{\nu}$  denotes the local Reynolds number.

### Solution of the problem

The PDEs system describing the above model is transmuted into an ODEs system by using suitable similarity variables. These ODEs system is handled by Runge-Kutta 4th order (RK-4) numerical method. Generally RK-4 method is most familiar. It is easy to implement, self-starting, and very stable method. The numerical solution for the problem is done by taking fixed values of similar variables  $\epsilon = 0.3, Pr = 1.5, K = 0.2, Ec = 0.8, \delta = 0.5, Nt = 0.3, Rd = 0.5, B = 1.0, \delta_T = 0.8, m = 0.5, Nb = 1.0,$  and  $Le = 0.7$ . This estimation is needed to provide one of the solution for PDEs, otherwise the PDEs are very difficult to tackle. The procedure for solving the problem is

$$p_1 = f, p_2 = f', p_3 = f'', p_4 = f''', pp_1 = f^{(iv)}, p_5 = \theta, p_6 = \theta' \\ pp_2 = \theta'', p_7 = \phi, p_8 = \phi', pp_3 = \phi'', p_9 = h, p_{10} = h', pp_4 = h''.$$

The transformed ODEs are

$$pp1 = (\alpha_1 * p_1)^{-1} * (-2 * p_2 + (1 + K) * p_4 + p_1 * p_3 + 3 * \alpha_1 * p_2 * p_4 + (-9 * \alpha_1 - 3 * \alpha_2) * p_3 * p_3 \\ - (2 * \alpha_1 + \alpha_2) * \eta * p_3 * p_4 + 3 * p_3 * p_3 * p_4 * \beta - 2 * Ha_2 * p_2), \\ pp2 = (-3 * Pr) * (3 + 3 * \epsilon * p_5 + 4 * Rd * Pr)^{-1} * ((1 + K) * Ec * p_3 * p_3 + p_1 * p_6 + \delta * p_5 \\ + Nb * p_8 * p_6 + Nt * p_6 * p_6 + \frac{\epsilon}{Pr} * p_6 * p_6) \\ pp3 = \frac{-Nt}{Nb} * pp2 - Le * p_1 * p_8, \\ pp4 = 2 * (2 + K)^{-1} * (4 * K * B * p_9 + 2 * K * B * p_3 + 3 * p_2 * p_9 - p_1 * p_{10}),$$

subject to the boundary constraints

$$\begin{cases} p_2 = 1, & p_1 = 0, & p_5 + \delta_T * p_6, & Nb * p_8 + Nt * p_6 = 0, & p_9 = -m * p_3, & \text{as } \eta \rightarrow 0, \\ p_9 = 0, & p_3 = 0, & p_2 = 0, & p_5 = 0, & p_7 = 0, & \text{as } \eta \rightarrow \infty. \end{cases}$$

### Numerical results and discussion

In this research, the micropolar 3rd grade fluid flow past an exponentially stretchable sheet is studied. By understanding fluid flow assumptions, the mathematical model is constructed. Introducing the relevant similarity transformations, the system of PDEs is changed into ODEs. Equations. (12)–(15) along with the BC (16) is numerically solved by use of MATLAB. MATLAB software utilizes Runge-Kutta-Fehlberg fourth-fifth order shooting technique to give numerical solutions for BVP. The characteristics of pertinent parameters involved on the  $\phi(\eta), \theta(\eta), f'(\eta)$  and  $h(\eta)$  are examined through graphical portrayals.

Figure 2 underlines the influence of fluid variable  $\alpha_1$  on velocity distribution, which shows the growth of  $f'(\eta)$  as rising the parameter  $\alpha_1$ . Physically, the viscosity of the material lowers if a larger value of  $\alpha_1$  is considered because of that force between the adjacent layers reduces, so in this case velocity increases. Figure 3 is the visual portrayal of  $\alpha_2$  on velocity. It is visualized that for a higher value of  $\alpha_2$ , a decline is seen in the curve of velocity distribution. This parameter causes shear-thickening of the fluid and a rise in resistance, that reduces the boundary layer flow, and originates an decrement in the size of the momentum boundary layer width. Figure 4 visualized variation of parameter  $\beta$  on velocity field, a rise in the velocity distribution is witnessed for a higher value of  $\beta$ . Actually  $\beta$  is inversely related to the viscosity. For greater  $\beta$ , viscosity declines and thus velocity rises. Figure 5 shows characteristics of Hartmann number  $Ha^2$  on velocity distribution. It seems that velocity falls via larger Hartmann number. This is because, when magnetic field rises then Lorentz forces get stronger. Resistance

to fluid flow is now more than before thus velocity is lowered. This process assists in controlling the size of the boundary layer.

Figure 6 is describing that temperature of the fluid declines for boosting of  $Pr$ . Perceptions are that thermal boundary layer thickness appears to decline while the rising upsides of  $Pr$  are utilized. As a result, when the Prandtl number ascends, pace of thermal conductivity gets higher. In this way, with more noteworthy  $Pr$ , heat will disperse more rapidly from the sheet. As it's undeniably true that liquids having prevalent Prandtl number  $Pr$  will have lesser worth of thermal conduction. Therefore, Prandtl number is utilized to augment the cooling behavior in the flows. Heat exchange for different values of Radiation parameter  $Rd$  is presented in Fig. 7. A direct relation is witnessed between  $Rd$  and temperature distribution. It is concluded that with upper values of  $Rd$  results in enhancement of temperature distribution. In fact, asending value of parameter  $Rd$  means more heat is transferred to the fluid, that takes temperature distribution to go upward. Figure 8 is visual proof of the effects of micropolar parameter  $K$  on  $\theta(\eta)$ , which is an evident that  $\theta(\eta)$  is diminishing function of  $K$ . Figure 9 indicates the temperature  $\theta(\eta)$  for different  $Ec$  values. By boosting  $Ec$ , an elevation is seen in the temperature distribution. It transfers kinematic energy into inner energy by overcoming viscous fluid tension and converting it to heat. Higher values of the Eckert number enhance the system's kinetic energy, which raises the temperature. As a result, increased viscous heat dissipation causes both growing heat and rising temperature.

The role of the  $Le$  on  $\phi(\eta)$  is observed in Fig. 10. The Lewis number is stated as the rate of heat-to-mass diffusion coefficient. It is utilized to express the flow of liquid in which heat and momentum transfer occur simultaneously. The concentration distribution becomes steeper when Lewis number is increased. A bigger  $Le$  implies the lower  $D_B$  (as it can be seen in Eq. 17) which causes a shorter penetration depth for concentration boundary layer. Figure 11 illustrates impact of  $Nb$  on the concentration field. A rise in Brownian motion variable gives a fall in  $\phi(\eta)$  inside boundary layer. Furthermore, the progressing amounts of brownian motion coefficient reduces the micro-mixing of nanoparticles into the fluid's zone which diminishes the boundary layer thickness of concentration distribution. The consequences of  $Nt$  on  $\phi(\eta)$  is exhibited in Fig. 12. It is seen that dimensionless concentration increases due to thermophoretic parameter. The thermophoresis constant amplifies the thermophoretic force, resulting in the transfer of nanoparticles from warm to cool locations and an increment in nanoparticle volume. In Fig. 13, the impact of Microinertia density parameter  $B$  is seen on micropolar profile. The behavior of  $h(\eta)$  is decreasing for increasing values of  $B$ .

In Table 1, the impacts of  $\alpha_1$ ,  $\alpha_2$ ,  $\beta$ , and  $Ha^2$  are noticed on the skin-friction coefficient whereas keeping other parameters fixed. Fixed values used are  $\epsilon = 0.3$ ,  $Pr = 1.5$ ,  $K = 0.2$ ,  $Ec = 0.8$ ,  $\delta = 0.5$ ,  $Nt = 0.3$ ,  $Rd = 0.5$ ,  $B = 1.0$ ,  $\delta_T = 0.8$ ,  $m = 0.5$ ,  $Nb = 1.0$ , and  $Le = 0.7$ . It is seen that skin-friction coefficient shows decrement for any larger value of  $\alpha_1$ ,  $\alpha_2$ , and  $Ha^2$  and shows opposite behavior for a larger value of  $\beta$ . Because the viscosity at the surface of the sheet increases with the evolution of the material constant, the skin friction coefficient decrease. The skin friction coefficient increases as the shear thickening coefficient  $\beta$  increases the thickness of the boundary layer. Increasing the Hartmann number  $Ha^2$ , which refers to a significantly stronger axial magnetic field and an increment in magnetic Lorentz resisting forces in the  $x$ -direction has a significant impact on the magnitude of primary skin friction coefficient for all axial coordinate values.

In Table 2, the impacts of some of pertinent parameters are observed on the local Nusselt number, while keeping other parameters unchanged as  $m = 0.5$ ,  $B = 1.0$ ,  $\alpha_2 = 0.5$ ,  $Ha^2 = 0.3$ ,  $\delta_T = 0.8$ ,  $Le = 0.7$ ,  $\beta = 0.5$ , and  $\alpha_1 = 0.1$ .

It is seen that Nusselt number gives a rise in its values as a larger value of  $Pr$ ,  $K$ ,  $Ec$ ,  $Rd$ ,  $\delta$ , and  $Nt$  is used while Nusselt number shows a decline for higher input of  $\epsilon$ . The increment in the values of Prandtl number cause a decline in the thermal diffusivity, and hence resist the rise in heat transmission rate at the boundary. Boosting the Prandtl number raises the average Nusselt number at the heated surface. Higher values of the  $Rd$  improve convective heat transmission which ultimately raises the average Nusselt number.

In Table 3, the behavior of local Sherwood number is observed for some of physical parameters involved. The following parameters are taken as unchanged in this course  $\alpha_1 = 0.1$ ,  $\delta = 0.5$ ,  $B = 1.0$ ,  $\alpha_2 = 0.5$ ,  $Pr = 1.5$ ,  $Ha^2 = 0.3$ ,  $\beta = 0.5$ ,  $\delta_T = 0.8$ ,  $\epsilon = 0.3$ ,  $Pr = 1.5$ ,  $K = 0.2$ ,  $Ec = 0.8$ ,  $Rd = 0.5$ , and  $m = 0.5$ . It is seen that Sherwood number shows increment for bigger values of  $Le$  and thermophoretic parameter  $Nt$  and decrement for higher value of Brownian motion number  $Nb$ .

## Concluding remarks

Third-grade micropolar fluid flow is analyzed in this research article. An ODEs system is generated from the PDEs system by a similarity transformation and then analytically solved by the fourth-fifth order Runge-Kutta-Fehlberg strategy. Several graphs are presented for the temperature, velocity, concentration, and micropolar fields to observe the impact of different parameters on them. The impact of various parameters on Nusselt number, skin-friction coefficient, and Sherwood number is also concluded. The main findings are

- Velocity distribution  $f'(\eta)$  boosts with  $\alpha_1$ ,  $\beta$ , while it has opposite behavior for  $\alpha_2$  and Hartmann number  $Ha^2$ .
- Temperature distribution  $\theta(\eta)$  presents an increasing behavior for Radiation parameter  $Rd$ , and Eckert number  $Ec$ , while, the opposite behavior for  $Pr$ , and  $K$ .
- Concentration distribution  $\phi(\eta)$  shows diminishing behavior as we put a higher value of Brownian motion number  $Nb$  and  $Le$ . On the contrary, this has the opposite behavior for  $Nt$ .
- Micropolar distribution  $h(\eta)$  displays an opposite relation with microinertia density parameter  $B$ .
- Skin-friction coefficient goes on increasing for higher values of parameters  $\alpha_1$ ,  $\alpha_2$ , and  $Ha^2$  and shows opposite behavior for bigger values of  $\beta$ .

- Nusselt number shows an increasing behavior as larger values of parameters  $Pr$ ,  $K$ ,  $Ec$ ,  $Rd$ ,  $\delta$ , and  $Nt$  are used, while Nusselt number depicts a decline for higher input of parameter  $\epsilon$ .
- Sherwood number shows increment for bigger values of parameters  $Le$  and  $Nt$  and decrement for the higher value of parameter  $Nb$ .

## Data availability

All data generated or analyzed during this study are included in this article.

Received: 24 April 2022; Accepted: 24 August 2022

Published online: 16 September 2022

## References

1. Abbasbandy, S., Hayat, T., Mahomed, F. M. & Ellahi, R. On comparison of exact and series solutions for thin film flow of a third-grade fluid. *Int. J. Numer. Meth. Fluids* **61**(9), 987–994 (2009).
2. Hayat, T., Naz, R., Alsaedi, A. & Rashidi, M. M. Hydromagnetic rotating flow of third grade fluid. *Appl. Math. Mech.* **34**(12), 1481–1494 (2013).
3. Farooq, U., Hayat, T., Alsaedi, A. & Liao, S. Heat and mass transfer of two-layer flows of third-grade nano-fluids in a vertical channel. *Appl. Math. Comput.* **242**, 528–540 (2014).
4. Sinha, A. MHD flow and heat transfer of a third order fluid in a porous channel with stretching wall: Application to hemodynamics. *Alex. Eng. J.* **54**(4), 1243–1252 (2015).
5. Okoya, S. S. Flow, thermal criticality and transition of a reactive third-grade fluid in a pipe with Reynolds' model viscosity. *J. Hydrodyn. Ser. B* **28**(1), 84–94 (2016).
6. Hayat, T., Ullah, I., Muhammad, T. & Alsaedi, A. A revised model for stretched flow of third grade fluid subject to magneto nanoparticles and convective condition. *J. Mol. Liq.* **230**, 608–615 (2017).
7. Hayat, T., Qayyum, S., Alsaedi, A. & Ahmad, B. Mechanisms of double stratification and magnetic field in flow of third grade fluid over a slendering stretching surface with variable thermal conductivity. *Results Phys.* **8**, 819–828 (2018).
8. Ali, A., Mumraiz, S., Nawaz, S., Awais, M. & Asghar, S. Third-grade fluid flow of stretching cylinder with heat source/sink. *J. Appl. Comput. Mech.* **6**, 1125–1132 (2020).
9. Nazeer, M., Ali, N., Ahmad, F. & Latif, M. Numerical and perturbation solutions of third-grade fluid in a porous channel: Boundary and thermal slip effects. *Pramana* **94**(1), 1–15 (2020).
10. Chaudhuri, S., Chakraborty, P., Das, R., Ranjan, A., & Mishra, V. K. An analytical investigation of pressure-driven transport and heat transfer of non-newtonian third-grade fluid flowing through parallel plates. In Proceedings of International Conference on Thermofluids, 275–286. Springer, Singapore (2021).
11. Padhi, S. & Nayak, I. Computational analysis of unsteady mhd flow of third grade fluid between two infinitely long porous plates. In *Advances in Fluid Dynamics* 305–314 (Springer, Singapore, 2021).
12. Eringen, A. C. Theory of micropolar fluids. *J. Math. Mech.*, pp 1–18 (1966).
13. Guram, G. S. & Smith, A. C. Stagnation flows of micropolar fluids with strong and weak interactions. *Comput. Math. Appl.* **6**(2), 213–233 (1980).
14. Gorla, R. S. R. & Takhar, H. S. Boundary layer flow of micropolar fluid on rotating axisymmetric surfaces with a concentrated heat source. *Acta Mech.* **105**(1), 1–10 (1994).
15. Gorla, R. S. R., Mansour, M. A. & Mohammedien, A. A. Combined convection in an axisymmetric stagnation flow of micropolar fluid. *Int. J. Numer. Methods Heat Fluid Flow* **6**(4), 47–55 (1996).
16. Seddeek, M. A. Flow of a magneto-micropolar fluid past a continuously moving plate. *Phys. Lett. A* **306**(4), 255–257 (2003).
17. Abo-Eldahab, E. M. & Ghonaim, A. F. Radiation effect on heat transfer of a micropolar fluid through a porous medium. *Appl. Math. Comput.* **169**(1), 500–510 (2005).
18. Mohamed, R. A. & Abo-Dahab, S. M. Influence of chemical reaction and thermal radiation on the heat and mass transfer in MHD micropolar flow over a vertical moving porous plate in a porous medium with heat generation. *Int. J. Therm. Sci.* **48**(9), 1800–1813 (2009).
19. Turkyilmazoglu, M. Flow of a micropolar fluid due to a porous stretching sheet and heat transfer. *Int. J. Non-Linear Mech.* **83**, 59–64 (2016).
20. Khan, A. *et al.* Darcy-Forchheimer flow of micropolar nanofluid between two plates in the rotating frame with non-uniform heat generation/absorption. *Adv. Mech. Eng.* **10**(10), 1687814018808850 (2018).
21. Nadeem, S., Malik, M. Y. & Abbas, N. Heat transfer of three-dimensional micropolar fluid on a Riga plate. *Can. J. Phys.* **98**(1), 32–38 (2020).
22. Nadeem, S., Abbas, N., Elmasry, Y. & Malik, M. Y. Numerical analysis of water based CNTs flow of micropolar fluid through rotating frame. *Comput. Methods Programs Biomed.* **186**, 105194 (2020).
23. Waqas, H., Hussain, S. & Khalid, S. MHD boundary layer flow of micropolar fluids due to porous shrinking surface with viscous dissipation and radiation. *Nucleus* **57**(3), 76–80 (2021).
24. Zhong, X. Strong solutions to the Cauchy problem of two-dimensional nonhomogeneous micropolar fluid equations with non-negative density. *Dyn. Partial Differ. Eqs.* **18**(1), 49–69 (2021).
25. Tassaddiq, A. Impact of Cattaneo-Christov heat flux model on MHD hybrid nano-micropolar fluid flow and heat transfer with viscous and joule dissipation effects. *Sci. Rep.* **11**(1), 1–14 (2021).
26. Crane, L. J. Flow past a stretching plate. *Zeitschrift für angewandte Mathematik und Physik ZAMP* **21**(4), 645–647 (1970).
27. Brady, J. F. & Acrivos, A. Steady flow in a channel or tube with an accelerating surface velocity. An exact solution to the Navier-Stokes equations with reverse flow. *J. Fluid Mech.* **112**, 127–150 (1981).
28. Ahmad, S. *et al.* Computational analysis of the unsteady 3D chemically reacting MHD flow with the properties of temperature dependent transpose suspended Maxwell nanofluid. *Case Stud. Therm. Eng.* **26**, 101169 (2021).
29. Ahmad, S., Nadeem, S. & Khan, M. N. Mixed convection hybridized micropolar nanofluid with triple stratification and Cattaneo-Christov heat flux model. *Phys. Scr.* **96**(7), 075205 (2021).
30. Khan, M. N., Ahmad, S. & Nadeem, S. Flow and heat transfer investigation of bio-convective hybrid nanofluid with triple stratification effects. *Phys. Scr.* **96**(6), 065210 (2021).
31. Nadeem, S., Ahmad, S. & Khan, M. N. Mixed convection flow of hybrid nanoparticle along a Riga surface with Thomson and Troianslip condition. *J. Therm. Anal. Calorim.* **143**(3), 2099–2109 (2021).
32. Ahmad, S., Nadeem, S. & Khan, M. N. Enhanced transport properties and its theoretical analysis in two-phase hybrid nanofluid. *Appl. Nanosci.* **12**(3), 309–316 (2022).
33. Khan, M. N. & Nadeem, S. Consequences of Darcy-Forchheimer and Cattaneo-Christov on a radiative three-dimensional Maxwell fluid flow over a vertical surface. *J. Taiwan Inst. Chem. Eng.* **118**, 1–11 (2021).

34. Shi, Q. H., Khan, M. N., Abbas, N., Khan, M. I., & Alzahrani, F. Heat and mass transfer analysis in the MHD flow of radiative Maxwell nanofluid with non-uniform heat source/sink. *Waves in Random and Complex Media*, pp 1–24 (2021).
35. Ahmad, S., Nadeem, S. & Khan, M. N. Heat enhancement analysis of the hybridized micropolar nanofluid with Cattaneo-Christov and stratification effects. *Proc. Inst. Mech. Eng. C J. Mech. Eng. Sci.* **236**(2), 943–955 (2022).
36. Ahmad, S. *et al.* Analysis of heat and mass transfer features of hybrid Casson nanofluid flow with the magnetic dipole past a stretched cylinder. *Appl. Sci.* **11**(23), 11203 (2021).
37. Khan, A. A., Ahmed, A., Askar, S., Ashraf, M., Ahmad, H., & Khan, M. N. Influence of the induced magnetic field on second-grade nanofluid flow with multiple slip boundary conditions. *Waves in Random and Complex Media*, pp 1–16 (2021).
38. Ahmad, S. *et al.* Impact of Joule heating and multiple slips on a Maxwell nanofluid flow past a slendering surface. *Commun. Theor. Phys.* **74**(1), 015001 (2021).
39. Khan, A. A., Khan, M. N., Nadeem, S., Hussain, S. M., & Ashraf, M. Thermal slip and homogeneous/heterogeneous reaction characteristics of second-grade fluid flow over an exponentially stretching sheet. *Proceedings of the Institution of Mechanical Engineers, Part E: Journal of Process Mechanical Engineering*, 09544089211064187 (2021).
40. Awan, A. U., Riaz, S., Abro, K. A., Siddiqua, A. & Ali, Q. The role of relaxation and retardation phenomenon of Oldroyd-B fluid flow through Stehfest's and Tzou's algorithms. *Nonlinear Eng.* **11**(1), 35–46 (2022).
41. Awan, A. U., Riaz, S., Ashfaq, M., & Abro, K. A. A scientific report of singular kernel on the rate-type fluid subject to the mixed convection flow. *Soft Comput.* pp 1–11 (2022).
42. Hou, E. *et al.* Flow analysis of hybridized nanomaterial liquid flow in the existence of multiple slips and hall current effect over a slendering stretching surface. *Curr. Comput.-Aided Drug Des.* **11**(12), 1546 (2021).
43. Gaffar, S. A., Bég, O. A. & Prasad, V. R. Mathematical modeling of natural convection in a third-grade viscoelastic micropolar fluid from an isothermal inverted cone. *Iran. J. Sci. Technol. Trans. Mech. Eng.* **44**(2), 383–402 (2020).
44. Salawu, S. O., Fatunmbi, E. O. & Ayanshola, A. M. On the diffusion reaction of fourth-grade hydromagnetic fluid flow and thermal criticality in a plane couette medium. *Results Eng.* **8**, 100169 (2020).
45. Fatunmbi, E. O., Ogunseye, H. A. & Sibanda, P. Magnetohydrodynamic micropolar fluid flow in a porous medium with multiple slip conditions. *Int. Commun. Heat Mass Transfer* **115**, 104577 (2020).
46. Koriko, O. K., Oreyeni, T., Omowaye, A. J. & Animasaun, I. L. Homotopy analysis of MHD free convective micropolar fluid flow along a vertical surface embedded in non-darcian thermally-stratified medium. *Open J. Fluid Dyn.* **6**(3), 198–221 (2016).
47. Fatunmbi, E. O., Adeosun, A. T., & Okoya, S. S. Entropy generation analysis in an unsteady hydromagnetic micropolar fluid flow along an exponentially stretchable sheet with slip properties. *Int. J. Modell. Simul.* pp 1–16 (2022).
48. Akbar, A. A. *et al.* Insight into the role of nanoparticles shape factors and diameter on the dynamics of rotating water-based fluid. *Nanomaterials* **12**(16), 2801 (2022).
49. Ibrahim, W. & Zemedu, C. MHD nonlinear mixed convection flow of micropolar nanofluid over nonisothermal sphere. *Math. Probl. Eng.* 2020 (2020).
50. Pakdemirli, M. The boundary layer equations of third-grade fluids. *Int. J. Non-Linear Mech.* **27**(5), 785–793 (1992).
51. Loganathan, K., Mohana, K., Mohanraj, M., Sakthivel, P. & Rajan, S. Impact of third-grade nanofluid flow across a convective surface in the presence of inclined Lorentz force: an approach to entropy optimization. *J. Therm. Anal. Calorim.* **144**(5), 1935–1947 (2021).
52. Chaudhary, S., Singh, S. & Chaudhary, S. Thermal radiation effects on MHD boundary layer flow over an exponentially stretching surface. *Appl. Math.* **6**(02), 295 (2015).
53. Sajid, M., Hayat, T. & Asghar, S. Non-similar analytic solution for MHD flow and heat transfer in a third-order fluid over a stretching sheet. *Int. J. Heat Mass Transf.* **50**(9–10), 1723–1736 (2007).

## Acknowledgements

The authors would like to thank the Deanship of Scientific Research at Umm Al-Qura University for supporting this work by Grant Code: 22UQU4331317DSR81.

## Author contributions

K.G.'s contributions are Resources; Software; Revision. N.A.A.'s contributions are Methodology; Resources; Revision. S.N.'s contributions are Concept; Revision; Software; Validation. E.M.T.E.D.'s contributions are Revision; Funding; Validation. A.U.A.'s contributions are Writing Manuscript; Supervision. M.F.Y.'s contributions are Revision; Formal Analysis; Restructuring.

## Competing interests

The authors declare no competing interests.

## Additional information

**Correspondence** and requests for materials should be addressed to A.U.A.

**Reprints and permissions information** is available at [www.nature.com/reprints](http://www.nature.com/reprints).

**Publisher's note** Springer Nature remains neutral with regard to jurisdictional claims in published maps and institutional affiliations.



**Open Access** This article is licensed under a Creative Commons Attribution 4.0 International License, which permits use, sharing, adaptation, distribution and reproduction in any medium or format, as long as you give appropriate credit to the original author(s) and the source, provide a link to the Creative Commons licence, and indicate if changes were made. The images or other third party material in this article are included in the article's Creative Commons licence, unless indicated otherwise in a credit line to the material. If material is not included in the article's Creative Commons licence and your intended use is not permitted by statutory regulation or exceeds the permitted use, you will need to obtain permission directly from the copyright holder. To view a copy of this licence, visit <http://creativecommons.org/licenses/by/4.0/>.

© The Author(s) 2022, corrected publication 2022